DESIGN AND FABRICATION OF TACTILE IMAGING METHOD FOR BREAST LUMP DETECTION

JOHNS HOPKINS UNIVERSITY

Whiting School of Engineering

Report submitted in fulfilment of class

Advanced Computer Integrated Surgery

By

Amrita Krishnaraj

MSE in Robotics

Mentors: Dr. Jeremy Brown, Dr. Nitish Thakor

May 2018

Table of Contents

Table of Contents

1.INTRODUCTION:

Reports of World Health Organization (WHO) indicated that cancers are among the main reasons of morbidity and death-rate worldwide. Moreover, they reported that in 2014, the new cases are around 14 million and the cancer related deaths are 8 million [1]. For 2018, there are estimated 2.6 million new cancer cases diagnosed and 0.9 million cancer deaths only in USA [2]. Unfortunately, the total number of new cases is expected to rise – for the next two decades – by about 70% [1]. Breast cancer disease is considered the second lethal killer among women all over the world [3]. Published statistics indicate that about 1 in 8 women will be harmed by this disease during their life [2]. It is believed that early detection tests for not only breast cancer but also all types of cancer save tens of thousands of lives yearly.

It is recommended that every post pubertal woman performs a self-exam monthly and has a clinical breast exam at least yearly. The existing screening methods available are MRI, Ultrasound, PET, Molecular based detection. But the golden method is the X-ray mammogram. Studies reveal that the X-ray mammogram causes exposure to low dose radiation which increase the risk of cancer by 40% in high risk individuals and by 8% for normal individuals [4]. Despite its limitations, and the fact that it is very uncomfortable (and even painful) for many women, mammography continues to be the most common screening tool used for breast cancer. Moreover, the sensitivity of breast self-examination (BSE) is as low as 20-30% [5]. This emphasizes a need for alternate simple and low-risk radiation methods.

Although breast cancer screening ideally involves information from both palpation and mammography, the information from the various imaging modalities is rarely assimilated. The way each modality is performed plays a large role in this. Clinical breast exams are performed by a clinician with the woman laying supine. Mammography, on the other hand, is performed by a radiologist with the woman standing. Combining the qualitative information from the ventral-dorsal plane with the more quantitative radiographic information obtained in an entirely different plane is difficult at best, and due to the different practitioners is not often done in a screening setting. Tactile imaging stands to bridge the gap between the two pieces of information, by providing a quantitative image of palpation that can be obtained in the same plane as a mammogram.

2.BACKGROUND LITERATURE:

The estimation of lesion parameters in tactile imaging has been explored most notably by Wellman [9] [10]. He assumed the model of a round lesion in a homogenous fatty tissue on a stiff substrate. Wellman showed that finite element analysis on the plane strain problem of the centerline can be used to accurately predict the centerline interfacial pressure distribution of spherical lesions. He used these two-dimensional finite element models to devise a tactile map feature-based algorithm to predict the diameter and depth of a very stiff lesion in soft tissue. His results were limited to lesions at least 100 times stiffer than the background fat, which applies only to cases of the stiffest cancers. Nevertheless, he showed that his algorithm's predictions are more accurate in determining the size of a stiff spherical region than manual palpation [10].

Weber [11] reproduced this work and attempted to find a more complete set of lesion parameters that includes the elastic modulus of a lesion of linear elastic material. His method was limited in accuracy, even with the input information of imager displacement, and the accuracy was dependent on the ratio of tumor modulus to background modulus. Both Wellman and Weber relied on fitting Gaussian curves to discrete-lump tactile maps in order to extract features useful for the inverse model Fig 1. Based on a Gaussian fit, they extracted base, amplitude, and standard deviation features.

Although this method has merit, as evidenced by the inverse models already established, it is limited in the features used to establish the inverse model, and potentially useful information is ignored in a Gaussian fit.

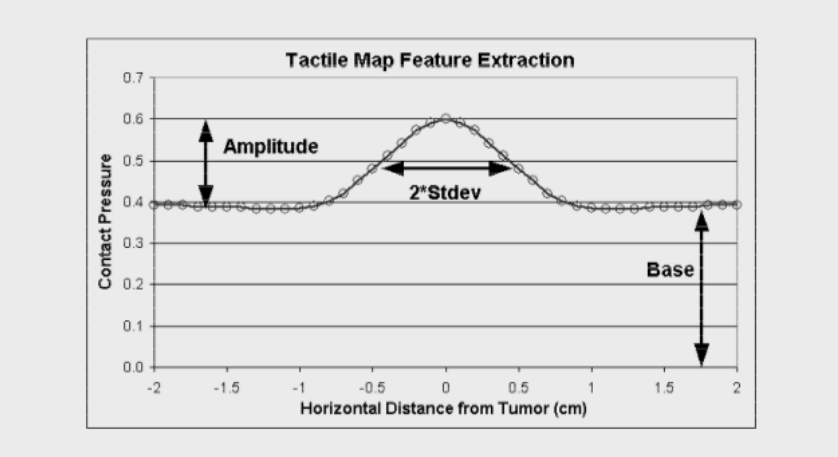

Fig 1. Centerline tactile map with estimated features

Sarvazyan et al [12] [13] have also studied the efficacy of tactile imaging in the detection of cancer, most notably in the prostate. The lesion-detecting algorithm they employ is based on different principles than the algorithms employed by Wellman and Weber. Sarvazyan [12] captures tactile data collected at different input forces and compares it to an expected anatomy-based map to pinpoint areas of mechanical heterogeneity in the organ. To date, the specific parameters of lesion size and elasticity modulus have not been an output of the algorithm employed. Rather, their work has shown that tactile imaging information can provide a Boolean assessment of whether each of the two lobes of the prostate contains a lesion more accurately than a digital rectal exam.

2.1 Tactile Imaging:

Previous studies on parameter estimation from Tactile Imaging were unable to accurately estimate lesion modulus. These earlier studies developed inversion schemes based on tactile maps, which spatially averages the tactile data to create a single image of the relative pressures collected as discussed in §1.1. This spatial averaging results in a loss of the detailed information found in separate pressure frames. In order to avoid the loss of information inherent in tactile mapping, we propose to develop an inversion algorithm based on a new tactile imaging modality called tactile scanning. The salient difference between tactile scanning and tactile mapping is that in tactile scanning all of the relevant information in the centerline of the pressure frames is used. The centerline is easily identified as the row or column with the greatest difference between its minimum and maximum values. In tactile scanning, each centerline pressure profile is merely concatenated to the previous pressure frames. The pressure profiles collected overlap spatially.

The data from tactile scanning is best visualized as a Composite Tactile Image (CTI). An example CTI for a single lump model is shown in Fig 2. The frames for this CTI were generated using finite element analysis, as will be detailed in the following section. This two-dimensional CTI is formed from the one-dimensional centerline pressure frames, collected every 2.5 mm for 80 mm centered at the lump. The pressure frames are stacked vertically, and the strong diagonal line of increased pressure attests to the symmetry of the imaged model.

It is important to note that in tactile imaging, the ends of the pressure frames will most likely not decrease to zero. Since the pressure sensors do not cover the entire surface of the imager, the

furthest extent of the imager that contacts the tissue is not covered with pressure sensors. This has the effect of cropping the pressure frames laterally to the width of the pressure sensor.

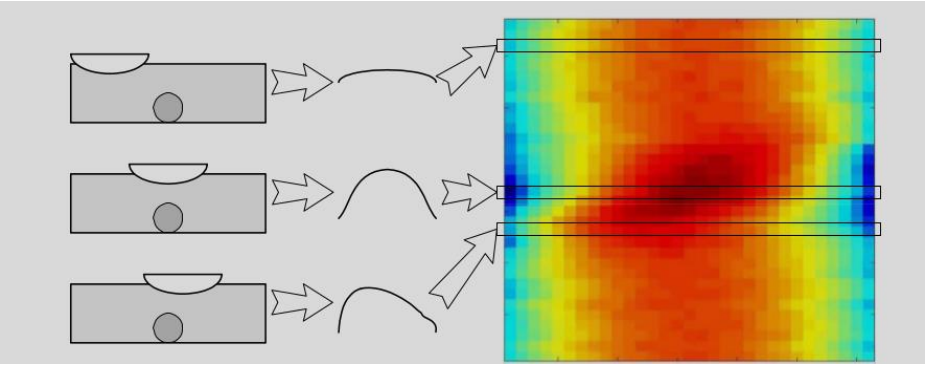

Fig 2. Information from tactile scanning transformed to composite image

3. PROJECT AIM:

The goal of the project is to develop a tactile imaging method for the detection of breast lumps. In tis work, we seek to come up with a method for estimating the underlying tissue parameters from the information collected during tactile imaging. The aim is to develop a tactile sensor for lump detection and custom measuring unit to work with the sensor. Further, algorithms to perform signal processing and to detect the lumps need to be developed. In addition, we aim to develop a way of determining the type of lump and creating a visual representation in accordance with clinical imaging methods. Finally, we aim to present the design of the interface garment or probe.

4. ANATOMY OF THE BREAST:

The human female breast, after puberty and before menopause, is made up of glandular tissue (the mammary glands), adipose tissue (fat cells), and supporting tissue (stroma, mainly collagen and elastin fibers). The general anatomy of the breast is shown in Fig 3**.** The glandular tissue, located in a cone with its apex at the nipple, is the site of milk production. The adipose tissue, in layers under the skin and above the chest wall, is the greatest contributor to the general shape and size of the breast. The supporting tissue is thin and sparse and affects mainly the gross appearance and motion of the breast. Menopause marks the conclusion of replacement of the glandular tissue by fat in a process called involution. Although there is a great variety in timing between individuals, involution of the breast begins at about 30 years of age and continues until menopause during a period called perimenopause. Involution manifests as the glandular component atrophies and is replaced in discrete sections by adipose tissue until the entire glandular component is replaced. The other components of the breast also undergo menopausal changes. Specifically, the volume of adipose tissue increases, while the elastic and collagen fibers weaken. Examination of the breast by palpation yields very different results depending on the relative age of the subject. A premenopausal breast has a high glandular tissue component under the superficial adipose tissue, leading to an inhomogeneous texture. Postmenopausal breasts, on the other hand, are far more uniform, and the adipose tissue is softer and easier to palpate in searching for stiff pathologies.

4.1 Mechanical Properties

Biological tissues are generally viscoelastic and strain-hardening [14], and the tissues found in the human breast are no exception. Under slow manipulation, however, (~1Hz) viscoelasticity effects are minimal [9] and can be ignored for all of the breast tissues in question. The supporting tissues plays a role when the breast is under tension, however under compression they offer negligible structural support, and naturally occupy such a small volume of the breast that their presence under compression can be ignored. Local mechanical properties, especially with the breast supported against gravity and examined in compression, are thus determined almost entirely by the glandular and adipose tissues. Adipose tissue exhibits linear elastic behavior through strains of 15% and in this linear regime has a Young's modulus of 15±4kPa. Glandular tissue exhibits linear elastic behavior through strains of 6% at a Young's modulus of 45±6kPa [15] [9].

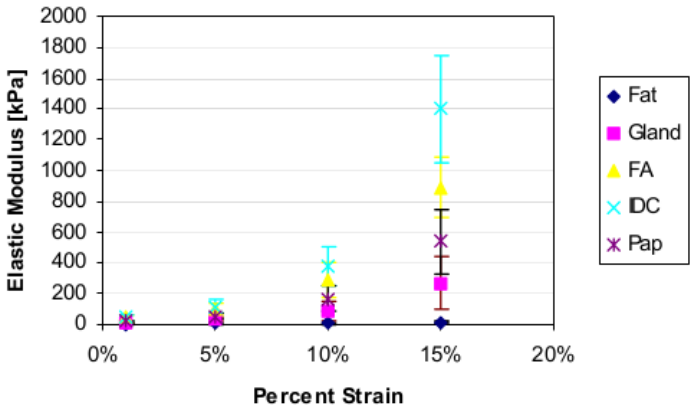

Fig 3. Breast cancer modulus variation

Pathological tissues are even stiffer than glandular tissues, and so can be felt as distinct under palpation, and viewed as stiffer in tactile imaging. The clearest distinction is made in postmenopausal breasts in which the background is almost entirely soft adipose tissue, however due to the distinct modulus, pathologies are often felt under palpation even in premenopausal breasts.

4.2 Breast Lumps:

The causes of palpable breast lumps can be broken down as follows [16]

fibrocystic changes 33%
no major pathology (i.e. normal) 24%
benign diseases 13%
cancer 23%
fibroadenoma 7%

It has been shown that a trained clinician can feel a lump as small as 3 mm in diameter [17] however the diagnostic ability of the CBE is highly dependent on the clinician administering the test. A proper CBE takes time and can make some patients and clinicians feel uncomfortable and is not often performed in full.

For idle cancer detection, it is mandatory to detect lumps as small as 3mm and at a depth of 10-12mm. The stiffness gradient of the palpable lumps varies with respect to the background tissues. Generally, the non-cancerous lumps are 6-8 times stiffer than the normal tissue and the cancerous lumps are 15-18 times stiffer compared to the normal tissues.

5. TECHNICAL APPROACH

A highly compliant fabric tactile sensor is designed which could be tailored into a garment or can be used as a probe. The changes in the tissue anatomy causes changes in the output voltage of the sensor which is then read out using an analog to digital conversion multiplexed readout circuit. The information forms the circuit is then processed in MATLAB. Thus, the system consists of four main modules, The tactile sensor, readout circuit, software processing and visualization. The data flow id as follows:

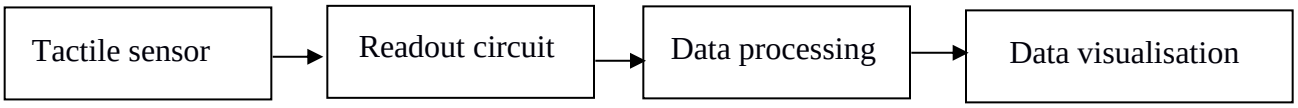

5.1 Sensor Design:

A specialized textile force sensitive resistor (FSR) was designed and built to measure applied forces during grasping tasks with a prosthetic hand. Based on previous work and a close collaboration with the Singapore Institute for Neurotechnology (SINAPSE), the textile force sensors are designed using several crossing traces of conductive fabric, which are separated by a piezoresistive textile layer. Fig. 4 shows the textile sensor cuff design in which flexible materials are used to allow the sensor to be placed on a prosthesis phalanx. A textile bi-directional stretch fusible interfacing serves as the foundation of the sensors. The conductive traces are used to sandwich a piezoresistive fabric layer, as mentioned, while an outer stretchy covering acts as a protective barrier between the conductive traces and the environment. The nature of the textile FSRs allows them to easily be fit on different regions of a prosthetic hand. The stretchable material that makes up each sensor cuff allows it to fit snugly against the surface of the prosthesis.

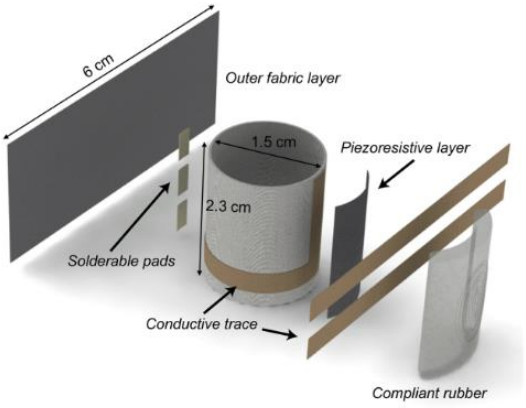

Fig 4. Figure of Sensor design

For this work we have created a 6 × *6* taxel sensor array using fabric-based materials. Fig. 5 illustrates the construction of the sensor. The transducer material consists of a piezoresistive fabric (LTT-SLPA, Eeonyx). Eight rows and columns of conductive fabric (Silver plated mesh, LessEMF) are arranged above and below the piezoresistive layer respectively. Fusible stretch interfacing made from

cotton (G785, Vilene) was fused onto the top and bottom of the sensor using an iron, thus holding the circuit together. The sensing area measures 7×7 cm. The spacing between the conductive elements was 0.5 cms and the width of the conductive fabric was 0.5 cms. This allows the sensor to measure lumps as small as 3 mm which is suitable for early stage lump detection.

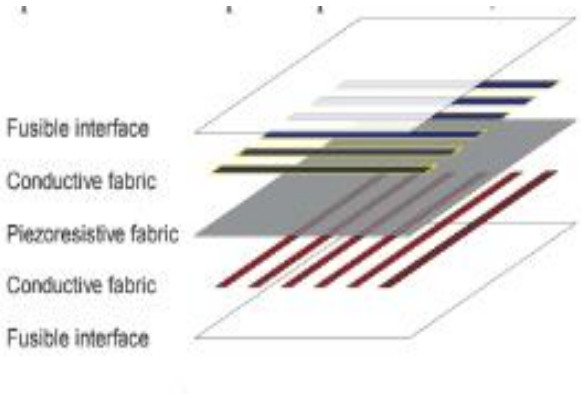

Fig 5. Multilayer sensor design

5.2 Sensor Characteristics:

The textile force sensitive resistors (FSRs) were characterized using an ADC (Arduino UNO). A normal force was applied directly to the sensing area of the textile cuff using a mechanical probe with a tip the same size as the sensing element a shown in Fig 6.

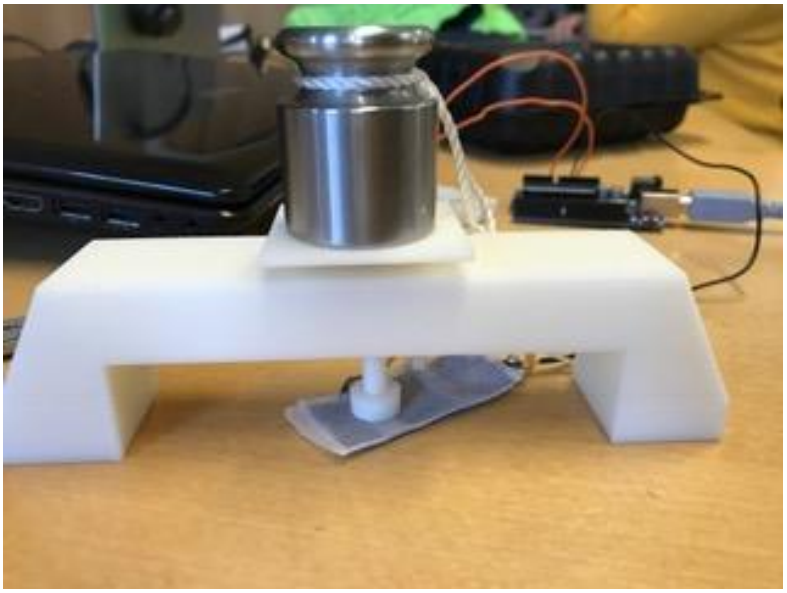

Fig 6. Calibration bridge and sensor loading

The applied force was measured using a USB electronic scale (RadioShack, Fort Worth, USA) with a range of 0-50 N and a precision of 0.01 N. Each sensor was tested 3 times at each applied load. Average sensor response was recorded and is shown in Fig. 6. Although each trace is cut to be 0.5 cm

in width, even slight variations can cause a change in the sensor response. As a result, the general trend for the sensors with a log-linear regression. The operating range for the sensors is defined as the linear section of the sensor response curve on a log-log scale, which was found to be 0.5–20 N. This can be fit using a power trendline of 7109.45 x $^{-1.3126}$ This operating range is comparable to force sensors that are available commercially.

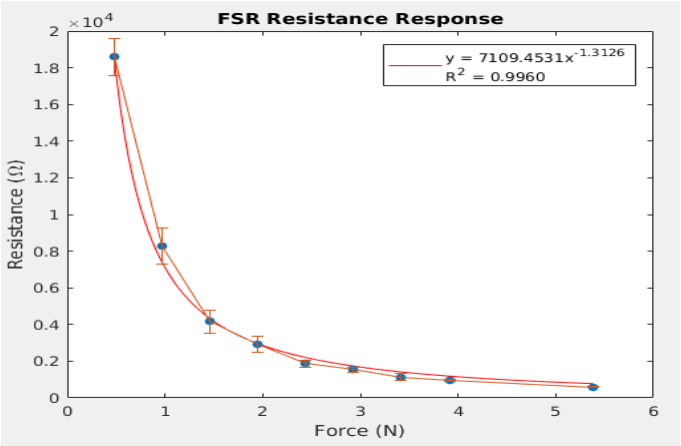

Fig 7. Sensor response curve

5.3 Readout Circuit

A standard multiplexed readout circuit was used (Fig. 6). The final sensor has 36 sensing points. As the resistance at each intersection decreases with increasing pressure, the pressure at each point is derived by measuring the potential difference across it. This is performed by activating each column *m* with a digital high signal (5V TTL) while deactivating other rows with a digital low. Each row *n* can then be read using a potential divider circuit, with each reading corresponding to the potential difference at point (*m*,*n*).

For this project, *Rdiv* = 10kΩ. A data acquisition board (16 bit, Arduino UNO) was used to provide excitation signals for the rows and perform analog-digital conversion (ADC) on the columns. The sampling rate was set to 1 kHz.

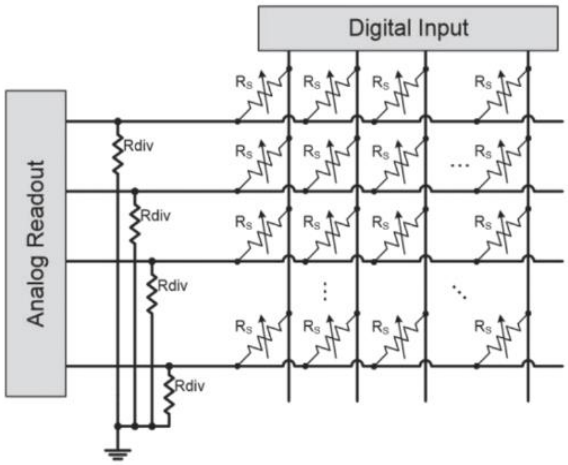

Fig 8. Readout circuit

5.4 Software Structure:

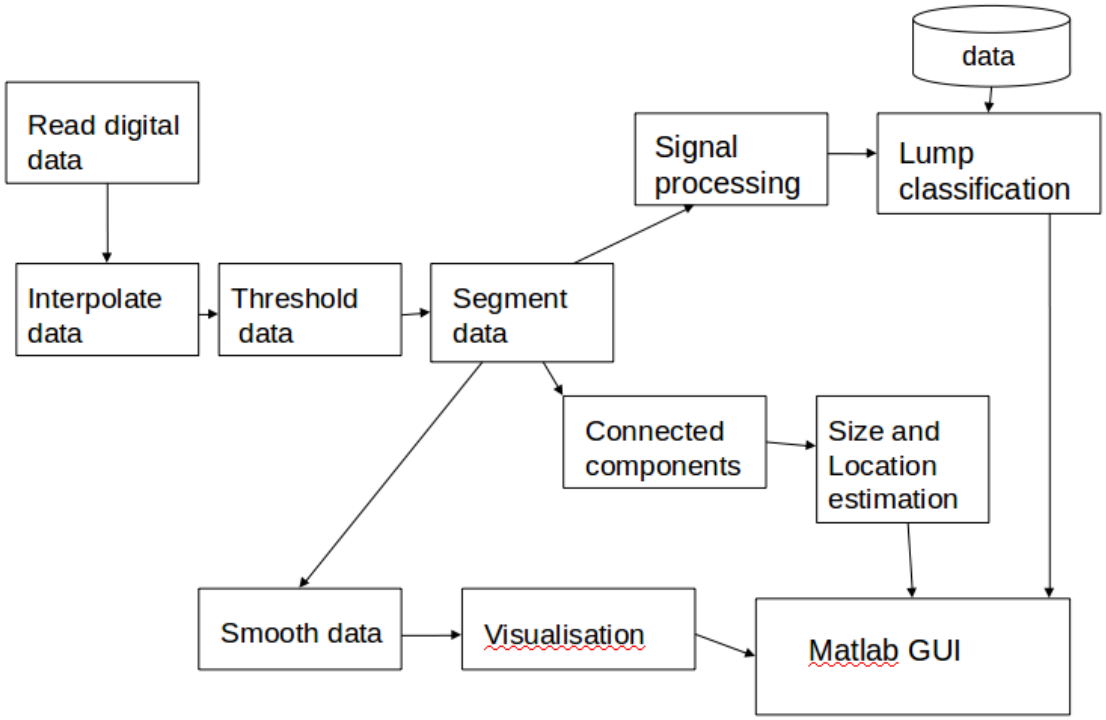

The captured data had spatial resolution of 5 mm (total 36 spatial samples, 6 × 6 array), and the captured data was smoothed via a moving average over ten frames of sensing data. To increase the contrast of the imaged lumps and render them more robust to differences in lump depth or loading, enhanced images were formed by interpolating the raw measurements. High resolution images were formed via linear interpolation, yielding values f (x, y) of the image at interpolated points (x, y) from those at measurement points (x_i, y_i), i = 1, 2, which are position coordinates of the sensing elements, and f (x_i, y_i), i = 1, 2, the measured values of voltage change. The final matrix obtained is a 11 x 11 array.

Subsequently using this data, otsu thresholding and segmentation was performed to obtain the enhanced image img(x,y). The obtained matrix is segmented into 4 different buckets. The threshold for each bucket was determined automatically by dividing the entire range into four quartiles based on the voltage distribution of the determined matrix.

Within-class variance is determined as the weighted sum of the variances of each cluster:

$$\sigma^2_{\text{Within}}(T) = n_B(T)\sigma^2_B(T) + n_O(T)\sigma^2_O(T)$$

Where, $n_B(T) = \sum_{i=0}^{T-1} p(i)$

$n_o(T) = \sum_{i=T}^{N-1} p(i)$

$\sigma^2_B(T)$ = the variance of pixels in background (other buckets)

$\sigma_O^2(T)$ = the variance of pixels in foreground (between thresholds of bucket)

The output from the otsu thresholding is a matrix with numbers from 1 to 4 depending on the voltage output. The number 1 represents the lowest voltage bucket which is the region that lumps are present. The bucket 2 contains second lowest set of voltage values which represents regions close to the lump where the tissue is affected. The bucket 3 represents the voltage set close to the normal tissue which could be harder tissues accounting for the tissue non-homogeneity. Bucket 4 contains the highest voltage range representing the normal tissue.

5.4.1 Lump localization:

Next step is to extract the connected components. 3-pixel neighborhood is used to find connected components. Two-pass Connected Component algorithm first labels all connected components with a unique label, and then unites some connected components together. The algorithm is the following:

Step 1) Set n = 0.
Step 2) For pixel img (x,y), define its 4 neighbors as pixels located at the
following locations (x,y),(x−1,y−1),(x,y−1),(x+ 1,y−1). If all of its neighboring pixels have value of 0, then increment the value of n by 1 and set img(x,y) to n. Otherwise, find the minimum non-zero value of its neighbors, and set img(x,y) to that value. Record the values of the neighbors into equivalence list.
Step 3) Repeat step 2 with the next pixel.
Step 4) After all pixels were processed and united into connected components, it is necessary to unite connected components using the equivalence list. Do a second pass on the image and unite all connected components.
Step 5) Re-label all connected components from 1 to the number of the components.

The matrix output from the connected components search is a matrix array with lumps numbered from 1 to the total number of lumps present. From the output of the connect component search, the location of the lump, filled in area and the centroids are determined using the inbuilt Matlab function regionprops. The entire matrix region is divided into 5 regions based on the breast segments. The nipple area is determined to be the circle with center as 2D midpoint(x_c,y_c) of the array and a radius of 2 pixels. The left top, right top, left down and right down segments are extended to the horizontal and vertical midpoints of the matrix.

5.4.2 Lump visualization:

Due to the construction of the sensor, the output from all the conducting strips are not identical. Due to this, the voltage from the no lump region is low to be classified in bucket 3. In order to overcome this effect, a background subtraction algorithm was developed. An unloaded senor is read and interpolated which now form the base image I(x,y). This image is used as reference and is compared to the segmented image img (x,y). The algorithm is as follows.

Step 1: Determine the first pixel with values 3 in img(x,y).
Step 2: For the pixel with value 3, compare the values f(x,y) with I(x,y). If the pixel difference is below the threshold and any neighboring pixel value is not lower than 3, make pixel (x,y) in img(x,y) as 4.
Step 3: Repeat the same for the next pixel.

The output image will be a background subtracted matrix with pixel values 3 only if the region is close to the lump or if the difference between the voltage value of the pixel of the unloaded sensor

and the loaded sensor is higher than the threshold. This condition represents a very small lump or a lump at a deep region which causes concern and needs to be verified. A MATLAB GUI was developed to display the image along with the area, centers, segments of location and the number of distinct lumps present along with their types.

5.4.3 Lump texture determination:

The difference in stiffness gradient between the different types of lumps is used to classify the lumps. First, the depth of the lump is predicted from the output voltage using the SVM classifier.

In order to determine the stiffness of the lumps, two assumptions are made. Firstly, the sensor is attached to a rigid surface compared to the breast tissues and the force exerted on the sensor will be translated into displacement of the tissues. Second, the displacement of the region with the lump as a reaction to the force is the same as the displacement of a normal tissue. Under the assumptions, the first principles (Hook's law) is used to determine the stiffness of the lumps.

$F = k. X$

where k = stiffness of material
F = Force output from sensor
X = Displacement

This stiffness is compared with the base stiffness to determine the texture of lump. The algorithm is as follows:
Step 1: Determine the depth at pixel using SVM classifier.
Step 2: Using the depth and the force information, determine stiffness. If stiffness is 5-9 times the stiffness of normal tissue, classify region as benign. Else if the stiffness is 14 times or higher, classify as cancerous. Stiffness of 9 to 14 is classified as biased region.
Step 3: For lumps in the biased region, the historic lump occurrence percentage per segment is used to classify as benign or cancerous.
Step 4: Repeat the process for all pixels in buckets 1 and 2.

6. SIMULATED TISSUE SAMPLES:

To evaluate lump imaging with the developed soft tactile sensing system, we prepared a set of simulated tissue samples. These were modeled on mechanical and geometric properties of experimentally measured prostate tissue and tumors [6], [8]. and were like phantom tissues used in prior studies on mechanical imaging of lumps [7]. We fabricated simulated tissues with soft polymer (Ecoflex 00-30, Smoothon, Inc.; M100 modulus of 7 × 10 4 Pa). Samples included stiff lumps, in the form of solid balls (Young's modulus 5 ×10 10 Pa) of varying radius and flat plates of varying dimensions and shapes (rectangle and plus) for the experiments on lump imaging**.** This material is stiffer than a biological tumor, but it provides an appropriate contrast in stiffness to the soft polymer and facilitates comparison with results from prior literature. Simulated tissues were fabricated with dimensions of 6 cm (width) × 6 cm (length) × 2.8 cm(height). We fabricated an array of tissues that varied in the depth h from the sample surface to the top of the lump and the diameter d of the solid.

In this research, we selected different values of d in the experiment: d = 3,4,6,10,16,20 mm, which are in accordance with the range of observed breast tumor sizes. Five values of embedding depth h (the distance between the tissue surface and the top of the lump) were used: h =0, 2, 4, 6, 10 mm. In

total, we fabricated 9 distinct simulated tissue samples including lumps, and one blank tissue with no lump, all of which were used in experiments.

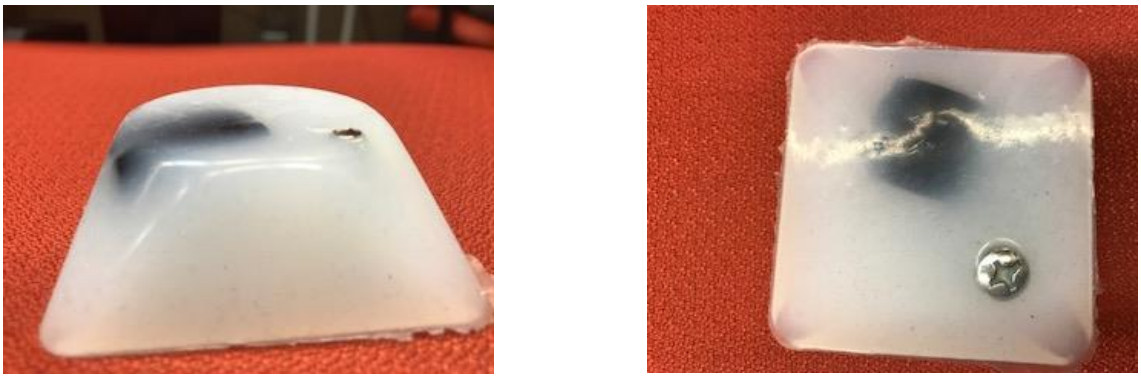

Fig 9. Breast tissue model and phantom

7. RESULTS:

When present, the lump was a prominent central feature in tactile images of all the samples that possessed it. The sensitivity of the sensor without application of any force was suitable up to a depth of 6-8mm. To cover the entire screening depth of 12 mm, a force of 1.5N is required. The sensitivity of the sensor with an applied 1.5N force is within the usable range up to a depth of 10mm. In order to capture the depth information and maximize the sensitivity, the region is scanned three times with forces 0N, 0.8N and 1.5N applied on the sensing elements.

For lump-containing tissues, as the lumps varied in depth, there was a decrease in voltage in the lump region of the image, and the decrease grew with increased embedding depth, yielding a qualitatively clearer image for lumps that were closer to the surface. The result of screening are shown in the figures below

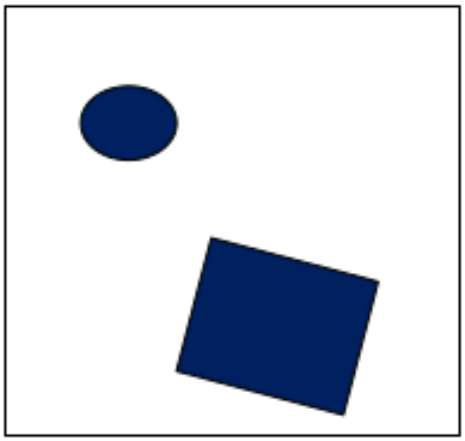

Fig 10. The top view breast phantom with the lumps present.

The circular object had the diameter d = 10mm and a depth h=3mm. The square object was a size of 20x20mm and at varied depths of d = 3 to 8mm. The object was scanned by three iterations with different force profiles 0, 0.8 and 1.5N. The result of the imaging is shown in Fig 9. The image shows a clear lumps area as the force applied increases as the sensor moves closer to the lump.

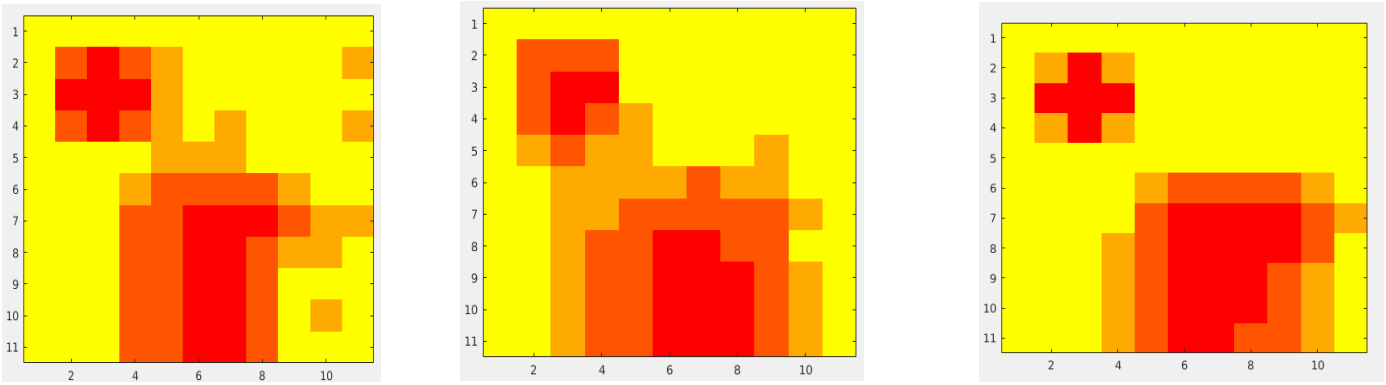

Fig 11. Image plots with different force applied. From left to right 0, 0,8 and 1.5 N.

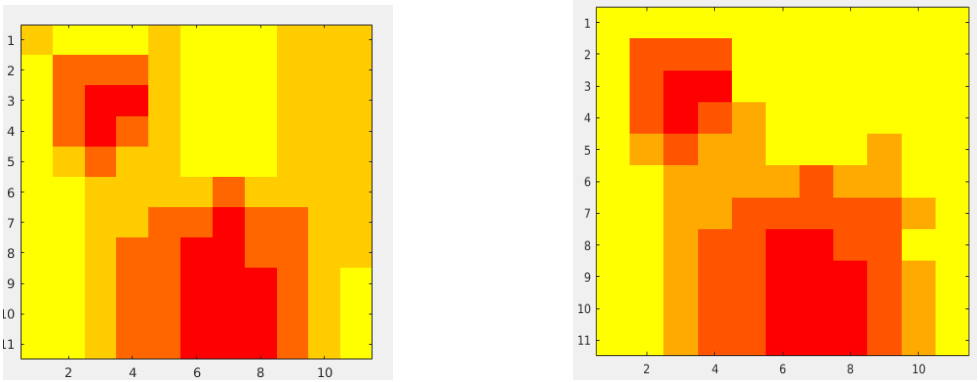

Fig 12. The left is the plot before background subtraction and the right is after background subtraction. The background subtraction provides a clearer visual representation of the lump

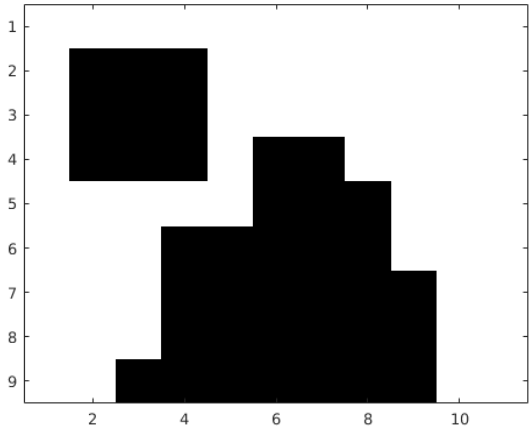

Fig 13. A binary image of the lump region consisting all voltage buckets except 4 (Normal tissue)

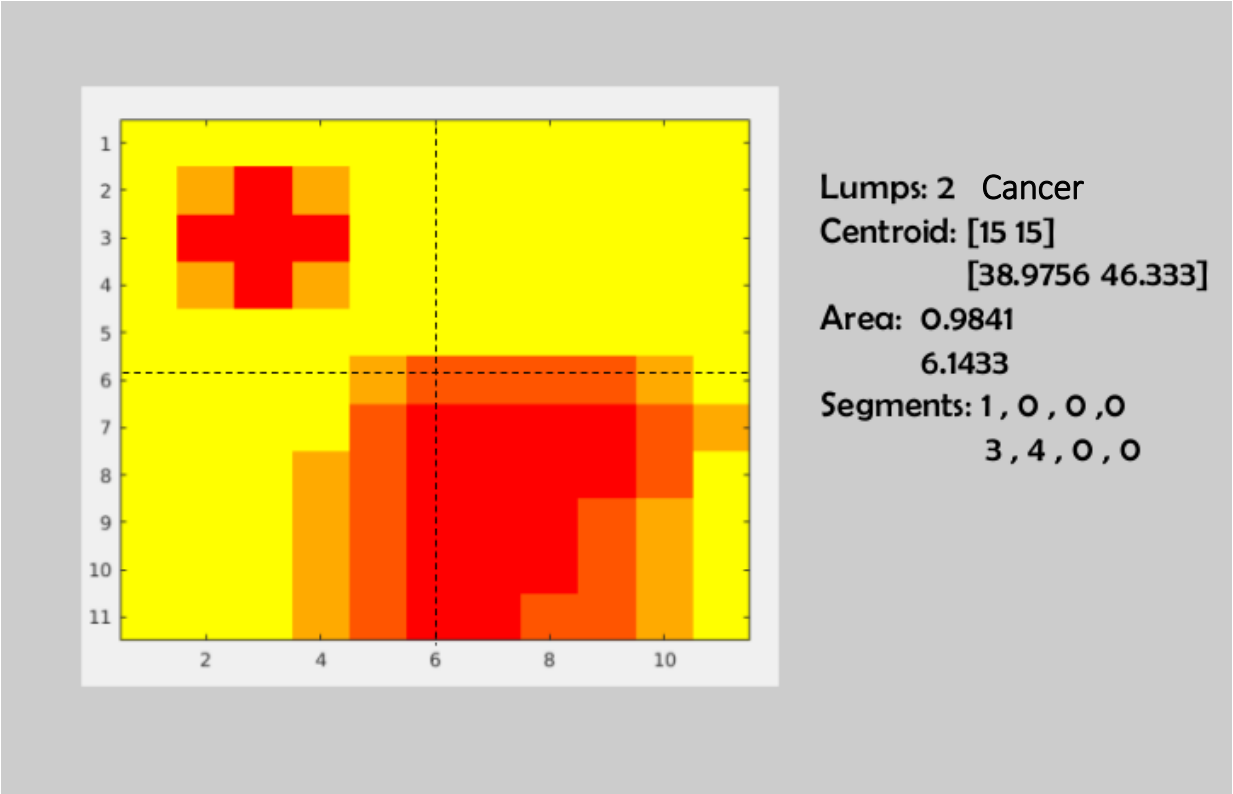

Fig 14. Matlab GUI representation of the lump region and its location in the breast

The phantom shown in Fig 13 consists of a flat plat of the shape shown in figure. The size of the bounding box of the lump is 30x20mm and plaed at a depth h = 10mm.

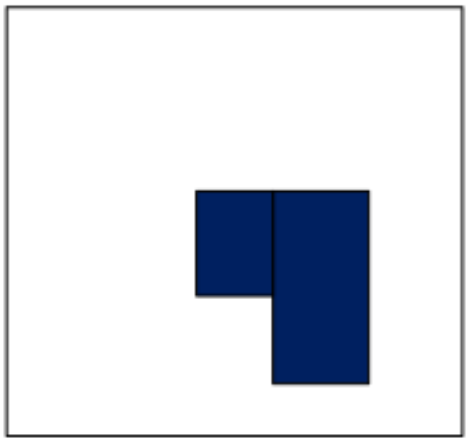

Fig 15. Top view of breast phantom with lumps present

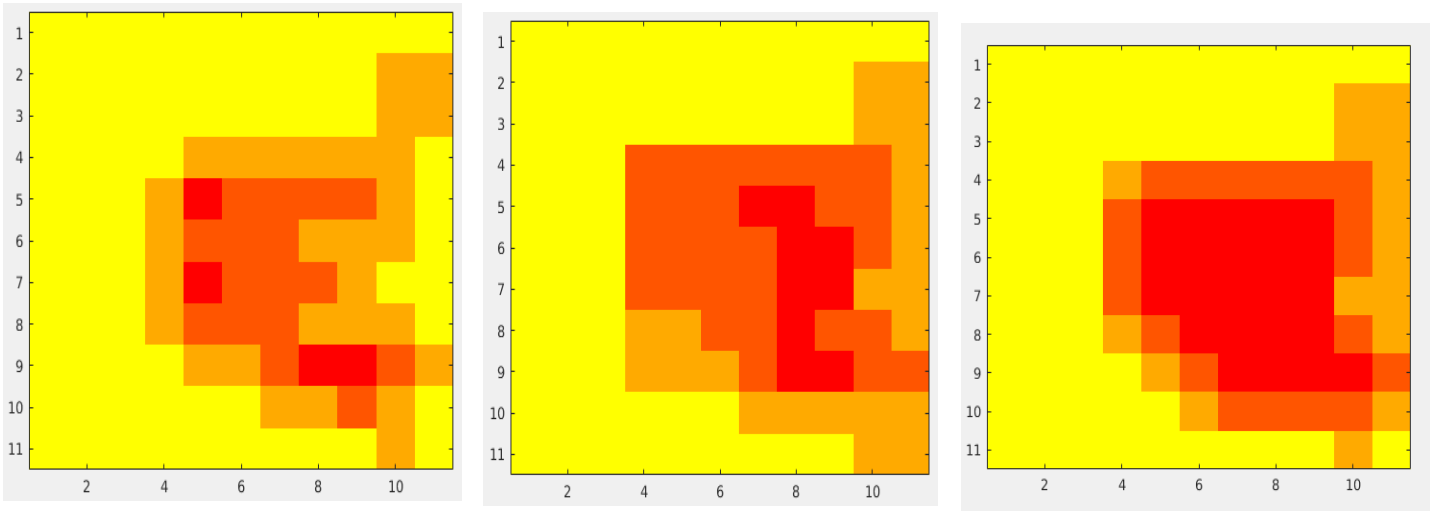

Fig 16. Image plots with different force applied. From left to right 0, 0,8 and 1.5 N**.**

The below table shows the relative stiffness of the lumps with respect to the phantom calculated by the algorithm.

Materials	Stiffness	Ratio
Plain phantom	0.0123	
Plastic	0.1677	13.64
Circle	0.1983	16.12
Plastic (Fig 13)	0.1399	11.38

Experiments were conducted with phantoms by varying the depth and the size to determine the accuracy. The sensitivity of the developed method is 83% for lumps below 6mm depth and from 8 to 10 mm, the sensitivity is 45% for the lump size of 8mm. The experiments were repeated by varying the size of the lumps. For lumps larger than 4mm, the success rate is 67% up to a depth of 6 mm and for smaller lumps, the success rate of detection falls to 54% still a rate higher than the CBE in most countries.

8. DISCUSSION:

The results of this research are promising, but there remain several limitations that may be improved upon in future work. Beyond a force of 1.5N, the sensor voltage output is extremely minimal for a large change in the voltage applied. The senor will not be able to measure the lumps due to saturation. This effect could be minimized using a lower resistor in the readout circuit. However, reducing the resistance will reduce the sensitivity of the output voltage at lower depths affecting the lump detection. The best way to overcome the limitations is to reduce the conducting strip width during construction of sensors.

One other limitation is the inability of the existing method to accurately measure both the stiffness and the depth of lump. Stiffer lumps at greater depths produce the same output voltage as less stiff lumps at lower depths. The different indentation forces applied have minimized the effect up to 8mm but beyond the depth of 8mm, the effect is uncertain and further experiments are required to warrant the accuracy of the developed methods.

While the processing presented here is quasi-static, the rate of change in the signals captured by the sensor (for example, the growth rate of contact area or strain energy density) is known to be salient to human stiffness perception. Such data could readily be captured dynamically in order to provide further information about the mechanical properties of palpated tissues. In human palpation, shear stress also plays an important sensory role, and could prove useful for mechanical imaging applications. The sensing method explored here proves adept at capturing stresses in the normal direction, and it may be useful to explore new features, comprising additional functional layers or structures, that could facilitate shear stress imaging. Tactile imaging can be effective at capturing lump geometry from surface measurements, but the three-dimensional, irregular nature of some tumors would pose significant challenges. Mechanically, if the sensor support is elastic, the geometry of the sensor can vary during palpation. Further investigation could be warranted to understand how this could affect sensor performance

Finally, to facilitate the translation of this work to applications in healthcare, experiments involving excised or in-vivo tissue samples would be especially valuable in order to establish a foundation for the clinical application of mechanical imaging with compliant tactile sensors.

9. FUTURE WORK:

The algorithms developed has good sensitivity up to a depth of 6mm. To improve the accuracy beyond 6mm, the algorithms could be implemented as two processes. Process 1 for up to a depth of 6mm and process two with otsu parameters tuned for a depth below 6mm. Further, experiments need to be conducted with different phantoms to determine the Type 1, 2 and 3 errors. The actual system to exert the forces needs to be developed as a phase two of the project to further validate the developed method. The developed system might affect the sensitivity of the developed algorithm. The developed method has allowance and parameter tuning will ensure sensitivity similar to the sensitivity demonstrated in experiments.

10. CONCLUSION:

This study investigated the utility of soft tactile sensors for imaging lumps in simulated tissue. Lumps manifested clearly in tactile imaging, even under gentle palpation, which is important in applications involving delicate or sensitive tissues. Using data from this system, and algorithms for extracting invariant signatures of subsurface lumps, we demonstrated that it is possible to robustly image such lumps. This could be done in a manner that is largely independent of the depth at which they are embedded, or the applied load. The study also provided preliminary data motivating the feasibility of tactile imaging with a wearable sensor.

11. MANAGMENT PLAN:

The initial aims of the project were to detect, localized the lumps and to determine the type of lump. Further, the maximum deliverable was to build a smart phone app to receive the data from MATLAB. However, along the course of the project, multiple steps that were not anticipated earlier were included to validate the developed method and to collect data for classifier. Hence the final deliverables were altered with the consent of the mentors. Also, multiple assumptions have been made which have to be warranted by in vivo experiments or substituted with classifiers with data collected during in vivo experiments.

The code, approach and the collected data has been shared with Neuro Engineering and Biomedical instrumentation Lab. A git repository has been created to avail the code for future reference. Weekly progress was updated with Dr. Jeremey Brown during Weekly meeting and changes to the project were made after discussion with mentor.

12. FINAL DELIVERABLE STATUS:

Minimum deliverables: Completed

The tactile sensor suitable for breast lump detection was developed and tested on phantoms with varying lump size and depth. A readout circuit was developed which was compatible with the sensor output and the post processing steps. An algorithm was developed to determine the location, area and size of the lumps from the sensor output.

Expected deliverables: Completed

An algorithm was developed to differentiate the different types of lumps. The developed algorithms use a classifier and to train the model, data was collected from different phantom models. Further, an algorithm was developed for visual representation of the lumps. Finally, a MATLAB GUI was developed to clinical data visualization and use by physicians.

Maximum deliverables: Partially Completed

The developed method was tested on newly produced phantoms and the sensitivity of the developed method was determined. Methods to improve accuracy was listed. The interface design and feasibility were detailed in the report and documented.

13. ACKNOWDELGMENT:

I would like to thank Dr. Jeremy Brown, my mentor for his support and guidance throughout the project. I would also like to thank Dr. Nitish Thakor, for giving me an opportunity to work with the sensor. Further I would like to thank Luke Osborn for his support and help with the experiments and understanding the sensor. Finally, I would like to thank Dr. Russell Taylor for the wonderful class and his guidance in finding the project.

REFERNCES:

[1]http://www.who.int/mediacentre/factsheets/fs297/en/

[2] http://www.cancer.org/research/cancerfactsstatistics/cancerfactsfigures 2018/

[3] H.D. Cheng, J. Shan, W. Ju, Y. Guo, L. Zhang, Automated breast cancer detection and classification using ultrasound images: a survey, Pattern Recog. 43 (1) (2010) 299–317.

[4] Eisenberg MJ, Afilalo JA, Lawler PR, Abrahamowicz M, Richard H, Pilote L. Cancer risk related to low-dose ionizing radiation from cardiac imaging in patients after acute myocardial infarction. CMAJ. 2011;182(4):430–436.

[5] https://jamanetwork.com/journals/jama/fullarticle/365753

[6] A. P. Astrand et al., "Detection of stiff nodules embedded in soft tissue phantoms, mimicking cancer tumours, using a tactile resonance sensor," J. Biomed. Sci. Eng., vol. 7, no. 4, pp. 181–193, 2014.

[7] J. C. Gwilliam et al., "Human vs. robotic tactile sensing: Detecting lumps in soft tissue," in Proc. IEEE Haptics Symp., 2010, pp. 21–28.

[8] V. Jalkanen et al., "Prostate tissue stiffness as measured with a resonance sensor system: A study on silicone and human prostate tissue in vitro," Med. Biol. Eng. Comput., vol. 44, no. 7, pp. 593–603, 2006.

[9]Wellman, P. S., Howe, R. D., Dewagan, N., Cundari, M. A., Dalton, E. P. and Kern, K. A., Tactile imaging: a method for documenting breast masses. First joint Biomed Eng Soc/IEEE Eng Med Bio Soc Conf. 1999.

[10] Wellman, P. S., Dalton, E. P. and al, e., "Tactile Imaging of Masses: First Clinical Report." Archives of Surgery 136(2): 204-8, 2001.

[11]Weber, G., Using Tactile Images to Differentiate Breast Cancer Types. Division of Engineering and Applied Sciences. Cambridge, Harvard University, 2000.

[12] Sarvazyan, A. P., Skovoroda, A. R. and Pyt'ev, Y. P., Mechanical introscopy - a new modality of medical imaging for detection of breast and prostate cancer. Eighth IEEE Symp. Computer Based Med. Sys. 1997.

[13] Sarvazyan, A. P., Computerized Palpation is more sensitive than the human finger. Proc 12th Int Symp on Biomedical Measurements and Instrumentation, Dubrovnik-Croatia. 1998.

[14] Fung, Y. C., Biomechanics: Mechanical Properties of Living Tissues. New York, Springer Verlag, 1993.

[15] Krouskop, T. A., Price, R. E., Wheeler, T. and Younes, P. S., Modulus Variations in Breast Tissues. 1st Int. Conf. On the Ultasonic Measurement and Imaging of Tissue Elasticity, Niagara Falls, ON, CA. 2002.

[16] Tavassolis, Atlas of Breast Pathology, 1996.

[17] Pennypacker, H. S. et at, "Why can't we do better breast examinations?" Nurse Prac. Forum 10(3): 122-8, 1999.

[18] L. Osborn, R. Kaliki, and N. V. Thakor," Utilizing tactile feedback for biomimetic grasping control in upper limb prostheses," in Proc. IEEE Int. Conf. Sensors, 2013, pp. 1266-1269.

[18] Tekscan, 2007, FlexiForce sensors. Available: http://www.tekscan.com/flexible-force-sensors

[19] W. Lee, J. Cabibihan, and N. Thakor, "Bio-mimetic strategies for tactile sensing," in I*EEE Sensors, 2013*. IEEE, 2013, pp. 1–4